nature cell biology

ARTICLES

Load-dependent kinetics of myosin-V can explain its high processivity

Claudia Veigel[1,3], Stephan Schmitz[1], Fei Wang[2] and James R. Sellers[2]

Recent studies provide strong evidence that single myosin class V molecules transport vesicles and organelles processively along F-actin, taking several 36-nm steps, 'hand over hand', for each diffusional encounter. The mechanisms regulating myosin-V's processivity remain unknown. Here, we have used an optical-tweezers-based transducer to measure the effect of load on the mechanical interactions between rabbit skeletal F-actin and a single head of mouse brain myosin-V, which produces its working stroke in two phases. We found that the lifetimes of the first phase of the working stroke changed exponentially and about 10-fold over a range of pushing and pulling forces of ± 1.5 pN. Stiffness measurements suggest that intramolecular forces could approach 3.6 pN when both heads are bound to F-actin, in which case extrapolation would predict the detachment kinetics of the front head to slow down 50-fold and the kinetics of the rear head to accelerate respectively. This synchronizing effect on the chemo-mechanical cycles of the heads increases the probability of the trail head detaching first and causes a strong increase in the number of forward steps per diffusional encounter over a system with no strain dependence.

Class V myosins are two-headed motor molecules that use the free energy from ATP hydrolysis to transport various cellular cargo, such as melanosomes or neuronal vesicles, along actin filaments[1–5]. Recent single-molecule studies[6–15] have shown that myosin-V is a processive motor that takes several 36-nm steps in a hand-over-hand fashion before detaching from its track. However, the detailed mechanism underlying such processive movement remains unclear. Here we address how load affects the kinetics of a single myosin-V head and provide evidence for a mechanical mechanism that couples the chemo-mechanical cycles of the two heads, increasing the processivity of the motor[16–18].

Myosin-V from mouse brain is composed of two heavy chains, each consisting of an amino-terminal head region forming the motor domain, a neck domain that binds six light chains, a carboxy-terminal tail region with coiled-coil motifs forming a dimerization domain and, finally, a cargo-binding domain[3,19]. Recent studies[6–14,20] suggest that during its ATPase cycle, one motor domain of the dimeric molecule first attaches to actin and generates force (leading into state A in Fig. 1A); at low load conditions this moves the centre of mass of the molecule towards the next actin binding site, where the free head can attach (state B). If this is followed by the detachment of the initially bound head to complete its chemo-mechanical cycle, force generated by the remaining bound head will move the molecule's centre of mass again forward (leading into state C, which is the same as state A with the heads exchanged). Repeating the above process will produce one forward step for each head completing its chemo-mechanical cycle. The processivity of myosin-V can be described quantitatively by the average number of chemo-mechanical cycles per diffusional encounter with actin. Assuming that the biochemical cycle of one head can be reduced to two states — attached to and detached from actin (Fig. 1B, a; ref. 21) — and that a single head spends about 70% of its biochemical cycle time attached to actin[22], we previously estimated that, for stochastically and independently cycling heads, myosin-V would remain bound to actin for on average of about eight biochemical cycles before detaching with both heads[13] (Fig. 1A; transition from state A to D). This is significantly less than the 20 to 60 processive forward steps reported for myosin-V in recent single molecule studies at low load conditions[6–11,13,14,23,24] and suggests some coordination of the two heads.

In addition, with both heads cycling independently in our simple model, the probability of either trail or lead head detaching first from the two-head-bound state is equal and half of the chemo-mechanical cycles in a 'processive run' are expected to be mechanically futile (as shown in Fig. 1B, b), because detachment of the lead head does not lead to forward movement (transition from state B to A in Fig. 1A). However, mechanical coupling of the two heads — for example, via a spring that becomes extended when both heads are bound (Fig. 1B, c, d) — could strongly increase the number of forward steps in a processive run (transition from state B to C in Fig. 1A). Intramolecular strain, imposing load in opposite directions on the heads, is expected to slow down the kinetics on the lead head by pulling it against its direction of motion, while accelerating the kinetics on the trail head by pushing it forward. The mechanical coupling should reduce the number of futile mechanical

[1]Physical Biochemistry, National Institute for Medical Research, The Ridgeway, Mill Hill, London NW7 1AA, UK. [2]Laboratory of Molecular Physiology, National Heart, Lung and Blood Institute, NIH, Bethesda, MD 20892, USA.
[3]Correspondence should be addressed to C.V. (e-mail: cveigel@nimr.mrc.ac.uk)

Published online: 14th August 2005; DOI: 10.1038/ncb1287

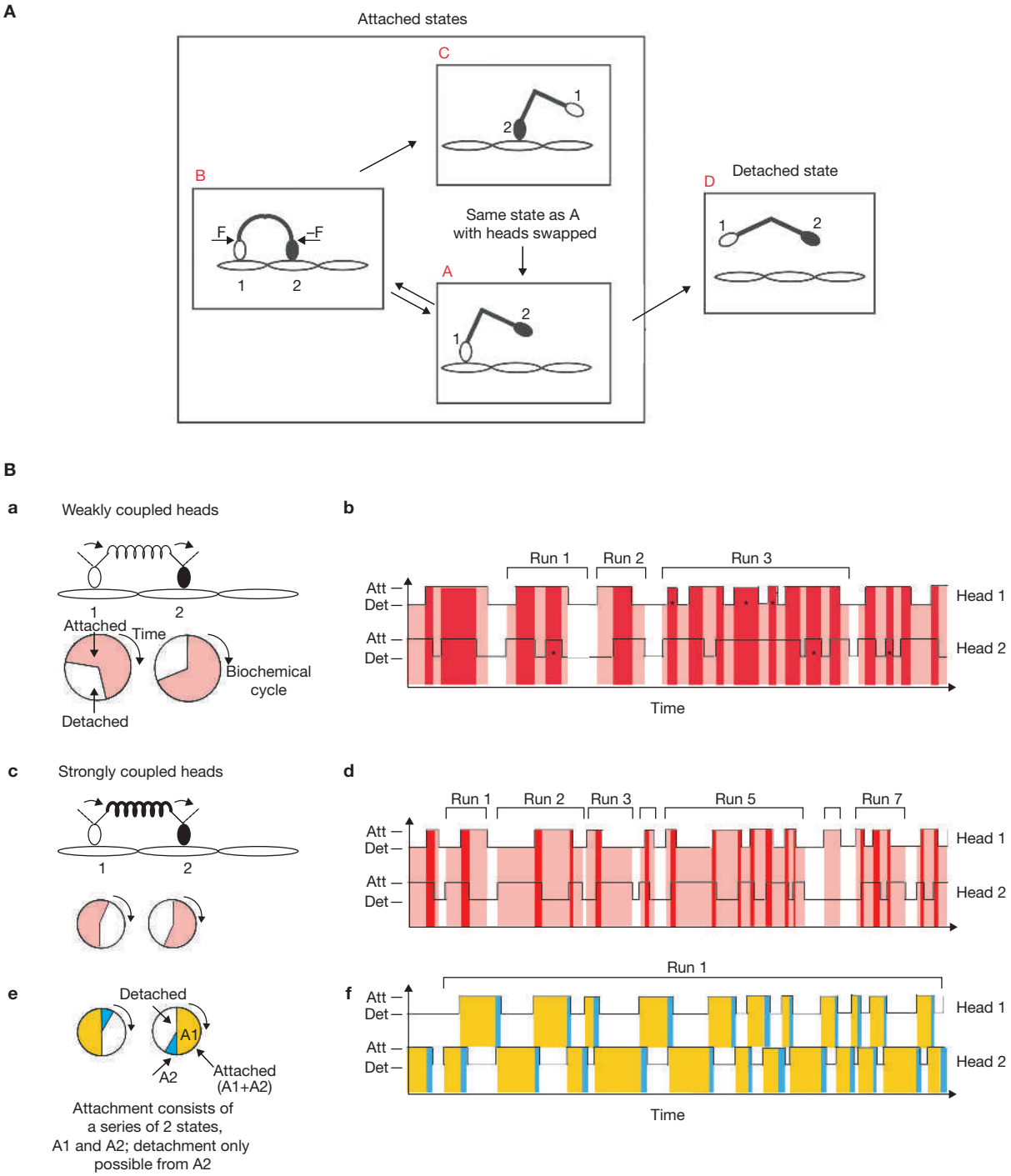

Figure 1 Intramolecular strain during processive movement. (**A**) The cartoon shows the bound configurations for myosin-V during processive movement. A single myosin head might adopt two states (detached from and attached to actin). A processive run starts in state A with a single head attached. Transition from state A to B and back to A, either directly (= futile in terms of forward movement) or via state C, continues the processive interaction. Transition from state A to D ends the processive run. State B is a strained state. (**B**) The cartoon illustrates the effect of mechanical coupling of the two myosin-V heads on processivity. (**a**, **b**) Simulation of acto-myosin interactions for independently cycling heads, connected via a very weak spring. Duty cycle ratio *r* (ratio between attached time and biochemical cycle time) is here ≈0.7 (ref. 22). (**b**) Time intervals are in white for both heads detached, in light red for one head attached, and in dark red for both heads attached; three processive interactions with different run lengths — including mechanically futile cycles (asterisks; detachment of lead head, see main text) — are observed. (**c**, **d**) Simulation for two heads mechanically coupled via a stiffer spring. The two-head bound state (dark red) is now strained and short lived. This causes: a reduction of the attached time for each head and therefore of the average cycle time per head (smaller circumference of the circles in **c**); increase in speed of processive movement (more runs per time in **d**); out-of-phase coordination of the two cycles; and reduction of the number of futile cycles. (**e**, **f**) The attached state consists of two successive states, only the second one (A2) leading into detachment. The lifetime of state A1 is strain-dependent and terminated by rebinding of the free head (blue on one head overlaps with yellow on the other head). The probability of a single bound head dwelling in state A2, from which it could detach (one head blue, the other head white), is minimized. This strongly increases the processive run length.

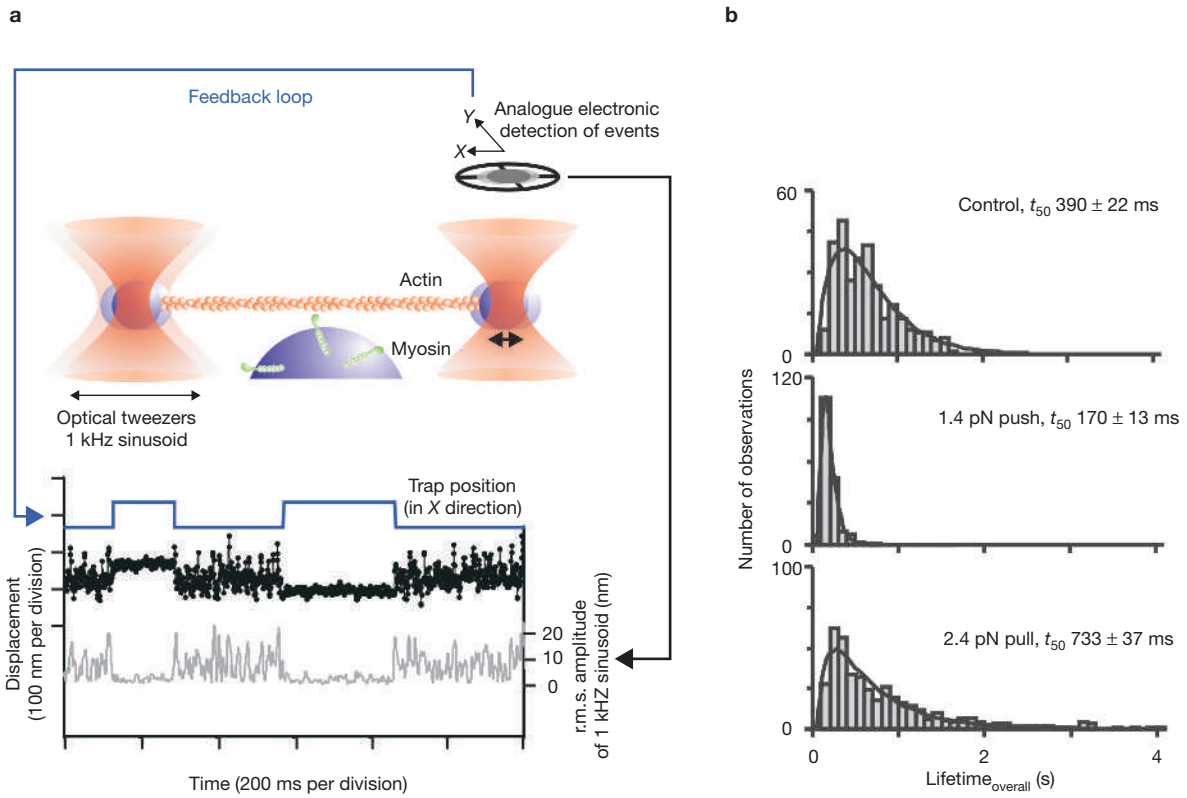

Figure 2 Effect of load on single molecule mechanical interactions measured for myosin-V S1 (MVS1). (**a**) The record shows bead position measured in parallel to the actin filament axis versus time (black data points). The position of one laser tweezer was oscillated at frequency $f = 1$ kHz and amplitude $A_0 = 35$ nm r.m.s. in order to detect myosin binding with millisecond time resolution. The transmission of this signal to the bead in the stationary tweezer was monitored (grey trace) so that the position of both optical tweezers could be moved rapidly (blue trace) to apply load to the bound crossbridge with a time delay of ~3 ms following detection of attachment (for details see Methods section and ref. 32). (**b**) Histograms of attached lifetimes measured at 3 μM ATP in absence or presence of applied load. Each histogram could be fitted by two exponential components, using rate constants k_1 and k_2 that had been determined independently for the two phases of the working stroke in Fig. 3b (for values see legend to Fig. 3). This is consistent with at least two sequential Poisson processes for the working stroke of MVS1.

cycles by increasing the probability that the trail head will detach first. This should also increase the speed of processive movement because the lifetime of the two-head-bound state is reduced (Fig. 1B, c, e; the total cycle time for one head, represented by the circumference of the circle, is reduced). If we assume in addition that the attached state of a single head is composed of a sequence of two states — A1 being strain dependent and, crucially, mostly terminated by rebinding of the free head, and only the second state, A2, leading into detachment — the average number of forward steps could be further increased. Premature detachment of a single bound head will now be reduced (Fig. 1B, e, f).

Recent single-molecule studies support the idea that the biochemical kinetics of myosin-V are regulated by load[6,7,13]. At low external loads and physiological concentrations of ATP, velocity of processive movement is limited by the rate of ADP release, presumably from the trailing head[7]; this rate is reduced by increasing load opposing movement. In contrast, at low ATP concentrations velocity is limited by the rate of ATP binding, which is relatively insensitive to external load[6]. In these experiments external load was acting simultaneously and in the same direction on each bound head, similar to the physiological effect that bound cargo would have on the processively moving motor. Independent of external forces, however, we suspect that there is another source of load that arises from intramolecular strain when both heads are bound to actin. The disparity between the 20–25-nm displacement produced by a single head[9,12,13,25,26] and the 36-nm binding distance between the heads of processively moving myosin-V implies intramolecular strain in the two-head-bound state. Consistent with this idea, we previously found that at physiological ATP concentrations and low external load, the rate-limiting kinetics of processively moving myosin-V were accelerated compared with the kinetics of a single head[13]. Recent modelling of solution kinetics[27] and of single-molecule fluorescence data characterizing processive run length of myosin-V[23] are consistent with the idea that intramolecular strain affects ADP release. To understand how the physiological combination of external forces and intramolecular strain regulates processive movement, we measured here the quantitative effect of pushing and pulling forces on the kinetics of force production by a single myosin-V crossbridge.

RESULTS

The actin-attached lifetime of myosin-V S1 is load dependent

We used an optical tweezers transducer[28,29] to characterize the mechanical properties of a single-headed myosin-V (MVS1)[30]. A single actin filament, suspended between two plastic microspheres held in two optical tweezers, was positioned over a third, surface-attached bead on which myosin-V was deposited at sufficiently low density for single molecular interactions of acto-myosin-V to occur. Mechanical interactions were measured by monitoring the positions of the microspheres holding the actin filament using two photodetectors[29] (Fig. 2a). To improve time resolution to detect myosin-binding events we applied a small-amplitude,

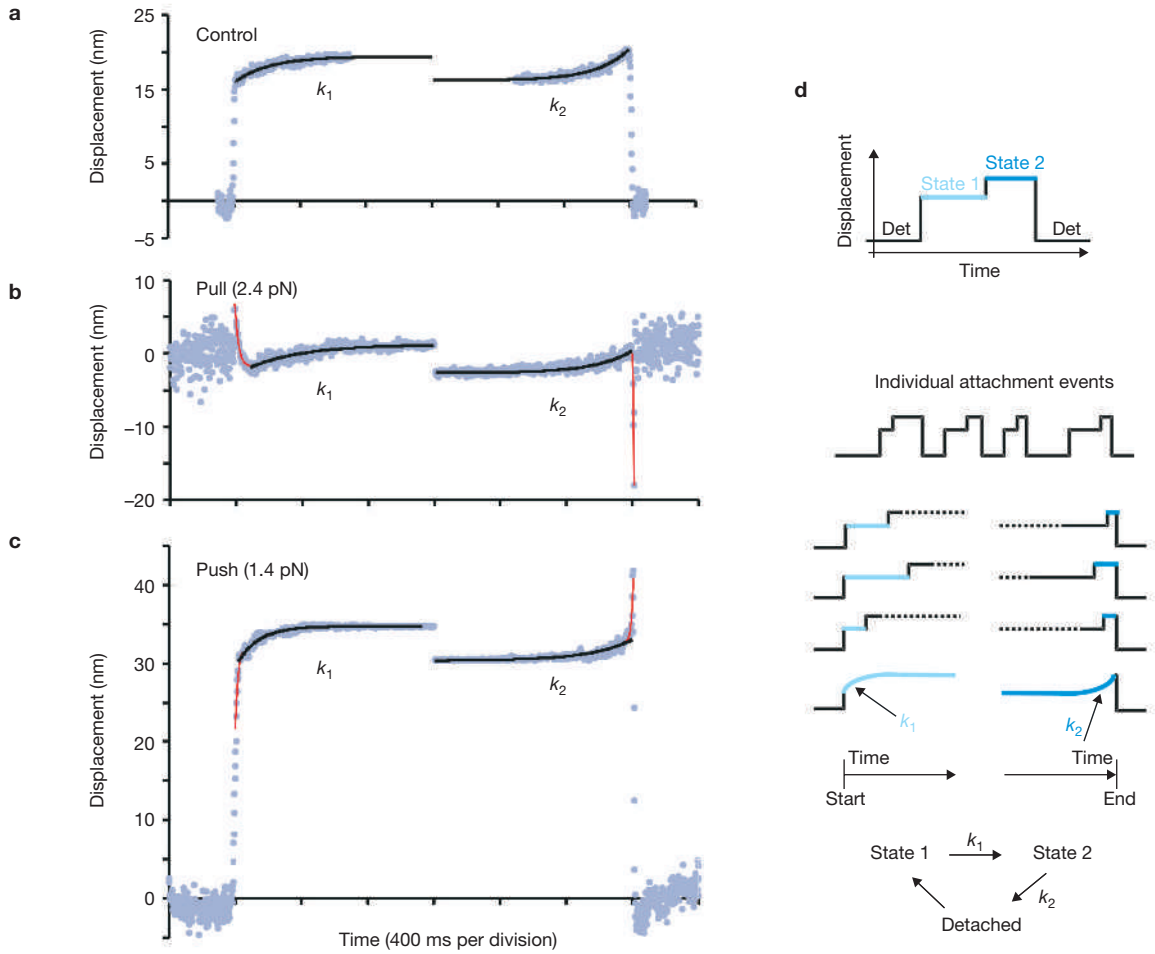

Figure 3 Load dependence of the two phases of the working stroke. Ensemble averaged attachment events measured at 3 μM ATP in absence (**a**) and in presence (**b**, **c**) of an applied force. Force was applied either in the direction of crossbridge movement (push) or against it (pull). (**d**) Attachment events were synchronized, either to the beginning or end of each event, and then averaged (blue data points = averaged data), as illustrated in the cartoon (see Methods and refs 13, 32). (**a**) Amplitudes and transition rates of phase 1 and 2 of the working stroke (k_1 and k_2) were determined by exponential fitting to the averaged data (solid black lines, see Methods and refs 13, 32), with $k_1 = 5\ s^{-1}$ and $k_2 = 5\ s^{-1}$. The red lines in **b**, **c** are fitted functions composed of two exponential components. The slower component is plotted on top of the red line as a solid black line. The fast component (visible red line) is explained by a passive, series elastic element in the system, as described in Methods and ref. 32. (**b**) Forward ensemble averaging: $k_1 = 3\ s^{-1}$ (black line), fast component = $46\ s^{-1}$ (red line). Backward ensemble averaging: $k_2 = 4.5\ s^{-1}$ (black line), fast component = $200\ s^{-1}$ (red line). (**c**) Forward ensemble averaging: $k_1 = 15\ s^{-1}$ (black line), fast component = $100\ s^{-1}$ (red line). Backward ensemble averaging: $k_2 = 8\ s^{-1}$ (black line), fast component = $160\ s^{-1}$ (red line).

high-frequency 'carrier' oscillation (1-kHz sinusoid) to one of the optical tweezers. Mechanical interactions of MVS1 with actin were identified by the change in amplitude of the 1-kHz sinusoid signal, transmitted to the bead in the stationary tweezers, corresponding to a sudden change in system stiffness as myosin bound to actin[31]. This enabled us to detect the onset of each binding event within ~1–2 ms. Monitoring the amplitude of this signal using an analogue electronic detection circuit we were able to rapidly apply a range of loads to the crossbridge and to investigate the effect of load on the kinetics during a single crossbridge cycle[32]. We found that the lifetimes of MVS1 interactions with actin are dependent on load. When no load was applied, MVS1 produced single isolated interactions with actin with an average lifetime (t_{50}) of 390 ± 22 ms (mean ± s.e.; see Methods, 3 μM ATP), similar to previous measurements at low-load conditions[13]. A push (in the direction of crossbridge movement) of 1.4 pN reduced the mean lifetime of attachments about twofold to 170 ± 13 ms. A pull (against the direction of crossbridge movement) of 2.4 pN had the opposite effect with the mean lifetime increasing almost twofold to 733 ± 37 ms. These result are consistent with at least one load-dependent transition during attachment.

The first phase of the working stroke is more sensitive to load than the second phase

Ensemble averaging of a large number of individual binding events, synchronized to the time points of their start or end, confirm that the working stroke of MVS1 is produced in two phases (Fig. 3a)[13]. Amplitude and transition rates of the two phases were determined by exponential fitting to the ensemble averaged data[13]. We previously found that the dwell time following the initial, 15-nm displacement (phase 1) was not affected by ATP concentration. In contrast, the dwell time following the second, 5-nm displacement (phase 2) became shorter at higher concentrations of ATP, suggesting that phase 2 is terminated when ATP binds to myosin, causing its detachment[13]. Here, we found that the rate constant k_1, which

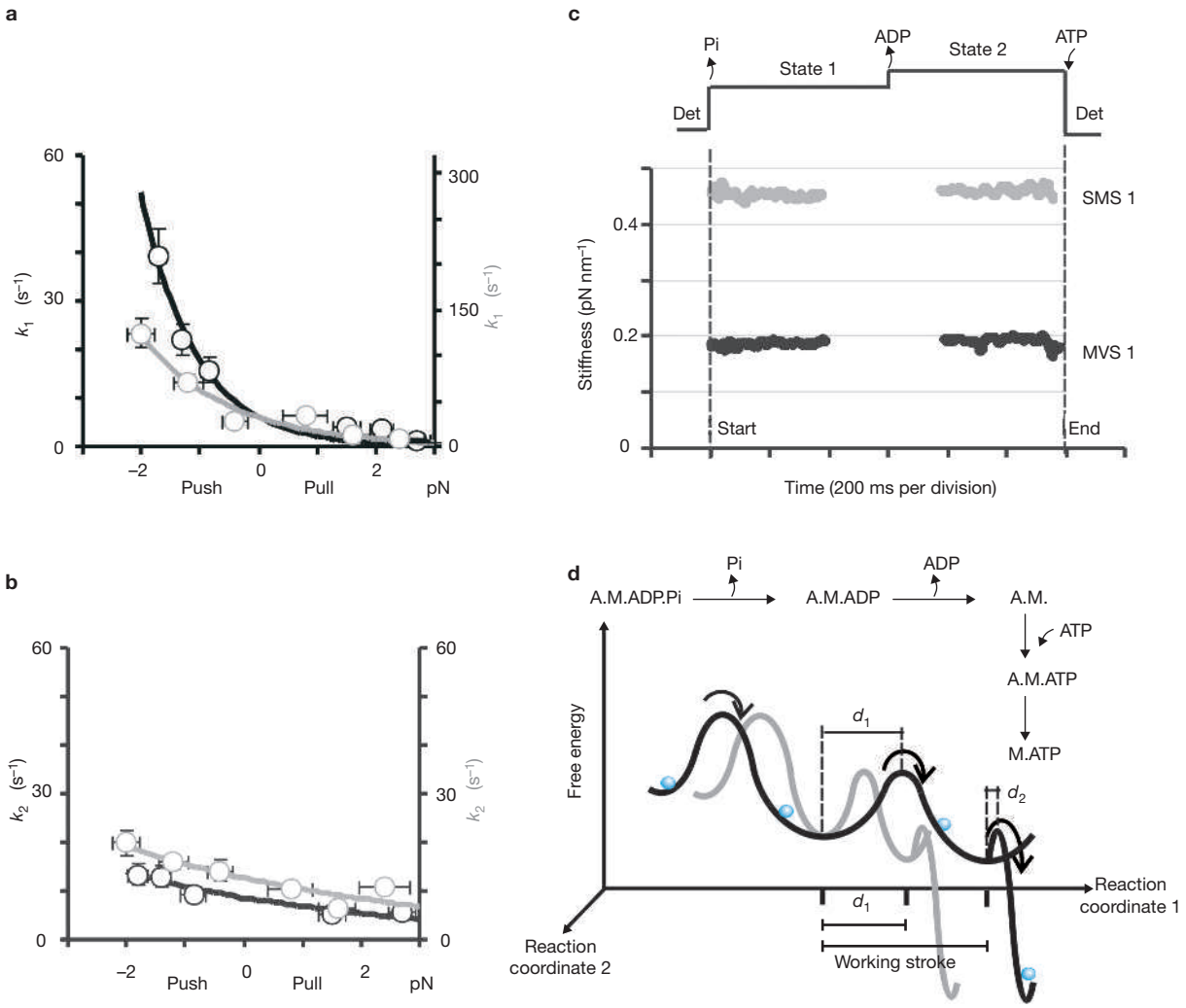

Figure 4 Load dependence of rates k_1 and k_2 for myosin-V and smooth muscle myosin. (**a**, **b**) Effect of force on the transition rates k_1 and k_2. For comparison, data for MVS1 are plotted together with data for previously characterized smooth muscle myosin S1 (SMS1)[32]. Circles and exponential fits are shown in black for MVS1 data, in grey for SMS1. Attachment events were ranked according to the individual load imposed on the crossbridge during attachment as described in the main text and ref. 32, and then grouped into six classes of load. k_1 and k_2 were then fitted to the ensemble average of each class. Number of events per class (from negative to positive forces) is 48, 68, 37, 29, 50 and 43. The plots in **a** could be fitted by a single exponential with $k_1 = k_0 \exp(-W/kT)$ and $W = Fd_1$; distance parameter, $d_1 = 4.3$ nm for MVS1 and 2.7 nm for SMS1 (ref. 32); rate for MVS1 and SMS1 in absence of applied load, $k_{01} = 6$ s^{-1} for MVS1 (fitting errors; standard error, s.e. = 0.4; regression coefficient, $r = 0.98$) and $k_{01} = 32$ s^{-1} for SMS1 respectively. The plots in **b** could also be fitted by a single exponential of the same form with distance parameter $d_2 = 0.9$ nm (fitting errors; s.e. = 0.12; $r = 0.92$) for MVS1 and distance parameter $d_2 = 0.8$ nm (fitting errors; s.e. = 0.1; $r = 0.91$) for SMS1. (**c**) Stiffness of a single attached crossbridge (MVS1 in black, SMS1 in grey). The stiffness was measured as described[29]. The time course of stiffness was calculated over a running time window of 30 ms. Measurements were performed at 3 μM ATP for MVS1 and at 20 μM ATP for SMS1. The average stiffness of acto-MVS1 was $\kappa_{MVS1} \approx 0.2$ pN nm^{-1} ($n = 54$). For acto-SMS1, $\kappa_{SMS1} \approx 0.45$ pN nm^{-1} ($n = 76$), similar to previous single molecule data on muscle acto-myosin in rigor state[29,40,41]. (**d**) Load-dependent change in a rate constant according to Arrhenius' transition state theory. The potential wells characterize the difference in free energy between adjacent biochemical states. Black lines characterize the energy landscape for MVS1 and grey lines for SMS1. For comparison, the curves for MVS1 and SMS1 have been arbitrarily aligned to the A.M.ADP state.

characterizes the lifetime of phase 1, increased from 5 ± 0.3 s^{-1} ($k_1 \pm$ s.e.m.; see Methods) to 15 ± 1 s^{-1} when the crossbridge was pushed by 1.4 pN (Fig. 3c), but slowed down to 3 ± 0.3 s^{-1} when pulled by 2.4 pN load in the opposite direction (Fig. 3b). The duration of phase 2 of the working stroke was much less strongly affected by the applied forces. The transition rate k_2, characterizing the lifetime of phase 2, increased from 5 ± 0.3 s^{-1} to 8 ± 0.6 s^{-1} when the crossbridge was pushed (Fig. 3c) and slowed down to 4.5 ± 0.4 s^{-1} when pulled (Fig. 3b). We conclude that force predominantly affects the transition rate k_1. We suspect this to be a nucleotide (probably ADP)-bound state because its dwell time is independent of ATP concentration.

We then grouped individual attachment events into six classes of load (Fig. 4) and fitted rate constants to the ensemble average for each class. The individual load during an attachment event was composed of applied load plus load caused by myosin binding to randomized positions along the actin filament, which moved thermally against the tweezers in between binding events[32]. The effect of a range of forces on k_1 can be described by a single exponential with $k_1 = k_{01} \exp(-W/kT)$ (rate at zero load $k_{01} = 6$ s^{-1}; $W = Fd_1$; F = total load on the crossbridge, distance parameter $d_1 = 4.3$ nm; kT = thermal energy), consistent with a strain-dependent transition over an activation energy barrier, as described by

Arrhenius' transition state theory[33] (Fig. 4a; black line). The effect of force on k_2 can also be described by a single exponential with $k_2 = k_{02}$ exp($-W/kT$) (rate at zero load $k_{02} = 8\ s^{-1}$; distance parameter $d_2 = 0.9$ nm) (Fig. 4b; black line).

Stiffness of acto-myosin-V S1 complexes

We measured the stiffness of acto-MVS1 complexes by oscillating the position of one laser tweezer at frequency $f = 100$ Hz, r.m.s. amplitude $A_0 = 70$ nm, while measuring the transmission of this motion to the bead in the other trap (Fig. 4c; ref. 29). We ensemble-averaged the time course of stiffness for individual acto-myosin interactions by synchronizing the interactions to the times of their start and end (Fig. 3; cartoon). An ATP concentration of 3 μM was chosen such that, on average, the acto-myosin crossbridges would spend about half of their attached lifetime in a nucleotide-bound state (phase 1 of the working stroke) and half in nucleotide-free rigor state (phase 2 of the working stroke). The data (Fig. 4c) show no changes in stiffness during the lifetime of acto-myosin interactions, and we conclude that the stiffness of acto-MVS1 during phase 1 and 2 of the working stroke is the same (average stiffness for acto-MVS1, $\kappa_{MVS1} \approx 0.2$ pN nm^{-1}; $n = 54$).

Load-dependent changes in rate constants according to Arrhenius' transition state theory

According to Arrhenius' transition state model, the kinetics of conformational changes involving activation energy barriers, such as those leading to production of force and movement in a molecular motor, are expected to be load-dependent[7,13,16,26,32,33]. We can summarize our findings on load-dependent kinetics of the working stroke and on myosin stiffness in a free-energy diagram (Fig. 4d). The biochemical states of the acto-myosin crossbridge cycle according to Lymn and Taylor[34] can be represented as parabolic potential wells in a free-energy landscape. The relative height of the potential wells characterizes the difference in free energy between adjacent states. The steepness of the potential wells is determined by the bending stiffness of the acto-myosin crossbridge along a particular reaction coordinate (here, coordinate 1 is the actin filament axis). The offset of the potential wells along one reaction coordinate describes the conformational changes (working stroke), associated with that transition. The transition between states involves an activation energy barrier. In absence of external force the forward rate constant from, for example, the acto-myosin-ADP state (A.M.ADP) to the nucleotide free rigor state (A.M) is described by $k_{01} \sim \exp(-\delta G/kT)$; where $\delta G = G_{activation} - G_{A.M.ADP} = 0.5[\kappa_{MVS1}(d_1)^2]$ (ref. 33). In the presence of force the transition rate is $k_1 = k_{01} \exp(-W/kT)$, with $W = Fd_1$ being the mechanical work done on the crossbridge via an external force F, d_1 = the distance parameter for that transition and kT = thermal energy. Black lines characterize the energy landscape for MVS1 and grey lines for smooth muscle myosin S1 (ref. 32) (SMS1) for comparison (see Discussion section). The distance parameter d_2 for the transition from the A.M state to the A.M.ATP state is very small. This indicates that the activation energy barrier for this transition is oriented mainly along an axis that is perpendicular to the reaction coordinate 1, along which we applied load.

DISCUSSION

Our data show that acto-myosin interactions of a single MVS1 head are dependent on load. The dwell time of phase 1, which follows the initial displacement of the working stroke, is particularly sensitive to load.

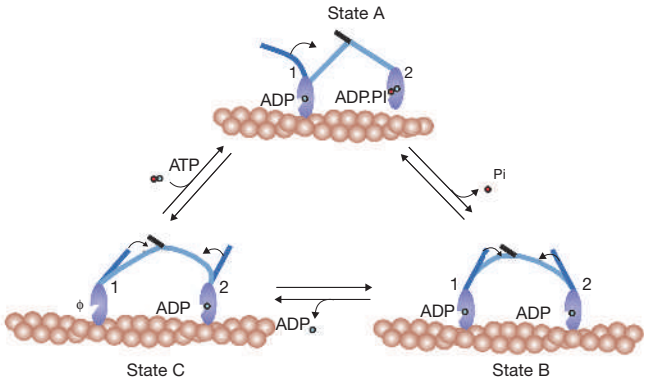

Figure 5 Model for processive movement of myosin-V along the 36-nm helical repeat of actin. Intramolecular strain upon binding of both heads affects the kinetics both of the leading and trailing head (leading head = head 2; trailing head = head 1).

The mechanical coupling of both heads in the dimeric molecule probably leads to coupling of their respective biochemical cycles through intramolecular strain. Because the working stroke (≈20–25 nm) produced by the initially bound head (Fig. 5; state A) is shorter than the binding distance of the heads in the two-head-bound state (36 nm), the free head has to diffuse over a distance of $d_{diffuse} \approx 10$–16 nm to the next binding site and binding of the free head will cause intramolecular strain (Fig. 5; state B). Knowing the mechanical properties of the system we can now estimate the kinetics for the rear and front head under the influence of strain. First, we can estimate the strain energy, U_s, from the stiffness of two MVS1s connected in series, to be $U_s = 0.5[(\kappa_{MVS1})/2][d_{diffuse}]^2 \approx 13$ pN nm $= 3\ k_bT$. The activation energy barrier, U_a, between phase 1 and 2 of the working stroke is found from the stiffness κ_{MVS1} and the distance parameter d_1, characterizing the load dependence of this transition, with $U_a = 0.5[\kappa_{MVS1}(d_1)^2] \approx 1.8$ pN nm $= 0.5\ k_bT$. Second, we expect intramolecular strain to affect the kinetics of the rear and the front head in opposite ways. Because a force $F \approx 1.6$ pN (with $F = \kappa_{MVS1}(d_{diffuse}/2)$) acts on the two heads in opposite directions, the detachment kinetics k_1 of the rear head are expected to accelerate by about fivefold (that is, by $\exp(Fd_1/k_bT) \approx \exp(0.5\ U_s/k_bT)$), whereas those of the lead head are expected to slow by about fivefold (that is, by $\exp(-Fd_1/k_bT)$).

We can now estimate the dwell time of the rear head, τ_{rear}, during processive movement. At saturating ATP concentration and low load, τ_{rear} is expected to be limited by the strain-dependent phase 1 of the working stroke, with $\tau_{rear} = 1/k_1 = [k_{01} \exp(Fd_1/kT)]^{-1} \approx 40$ ms. This is consistent with previous observations for the dwell times between steps during processive movement (≈ 60–70 ms)[6,7,13]. It is, however, significantly shorter than the dwell times for a single MVS1 head (≈ 110 ms)[13], suggesting that in these conditions the rate-limiting step of processive movement might be the strain-dependent detachment of the rear head.

The kinetics of the lead head, however, will also affect processive movement. Note that in the model described so far, we assume that the lead head has bound to actin, causing intramolecular strain, but has not yet produced the first step of its working stroke (Fig. 5; state B). It is not clear yet whether the lead head does proceed through the first step of the working stroke immediately after binding to actin or whether there is a load-dependent time delay, as has been suggested in electron microscopy studies[1,35]. We know that for a single head at low load this conformational change occurs within 1–2 ms after binding to actin (Fig. 3a),

too fast for its kinetics to be resolved in our experiments. Nevertheless, we can estimate the intramolecular strain that would be created once the lead head has produced this conformational change, with the rear head still bound. The N-terminal part of the lever-arm of both heads will then point in the same direction (Fig. 5; state C) and the strain energy will rise to up to $U_s = 0.5[(\kappa_{MVS1})/2)(36\ nm)^2 = 65\ pN\ nm \approx 16\ k_bT$. Each head will now experience a force with an absolute value of $F = \kappa_{MVS1}(36\ nm/2) \approx 3.6\ pN$. Extrapolating the load dependence of the kinetics, we would expect this force to accelerate the detachment kinetics of the rear head by about 50-fold compared with unstrained conditions (with $k_1 = k_{01} \exp(Fd_1/kT) \approx 300\ s^{-1}$), and to slow down those on the lead head to about one-fiftieth respectively (Fig. 4a). The rear head will now be able to bind ATP very quickly and, at saturating ATP concentrations, detach within only a few milliseconds. However, at saturating ATP and low load, the dwell times between processive steps are ≈ 60–70 ms[6,7,13], suggesting that the lead head might only produce the first step of its working stroke after some time delay. Therefore we suspect that at least two strain-dependent steps are rate limiting for processive movement of myosin-V; first, a strain-dependent transition on the lead head that produces a 20 nm working stroke associated with either Pi release or an ADP isomerization, and that is responsible for building up additional intramolecular strain; and second, a strain-dependent transition on the rear head that produces a 5 nm working stroke for the transition from phase 1 to phase 2 of the working stroke, coupled to either an ADP isomerization or ADP release. A recent solution kinetics study is consistent with ADP release accelerated two- to threefold on the trail head and slowed down about 50-fold on the lead head[27]. However, different parameters are measured in solution kinetics and mechanical studies, and combined single-molecule biochemical and mechanical studies are required to address these issues in more detail.

We compared the effect of load on rates k_1 and k_2 for MVS1 and smooth muscle myosin S1 (SMS1), which also produces its working stroke in two phases[32,36,37]. The effect on rates k_1 and k_2 is similar for both myosins; k_1 however is apparently more sensitive to load for MVS1 (Fig. 4a, b). This is described by the distance parameter d_1 (characterizing the slope in Fig. 4a), with $d_{1(MVS1)} = 4.3$ nm for MVS1 compared with $d_{1(SMS1)} = 2.7$ nm for SMS1, suggesting MVS1 to be about 1.6 times more sensitive to load. We also found a higher stiffness for acto-SMS1 with $\kappa_{SMS1}/\kappa_{MVS1} \approx 2.3$ (Fig. 4c). Values for distance parameter and stiffness suggest that the activation energy barrier for the transition from the ADP-bound state into rigor, $U_a = 0.5 \times \kappa(d_1)^2$, is similar for both myosins (Fig. 4d). If the acto-myosin compliance were dominated by bending of the light-chain binding domain[38], we would expect the measured stiffness to depend on the reciprocal of the cubed lever-arm length L, so that $\kappa_{(SMS1)}/\kappa_{(MVS1)} \approx L_{(SMS1)}{}^{-3}/L_{(MVS1)}{}^{-3}$ and $\kappa_{(SMS1)}$ to be 27 times $\kappa_{(MVS1)}$. This is assuming a similar bending stiffness of the light-chain binding domain per unit length for both myosins. Interestingly, the difference in stiffness was much less pronounced than that. This could be due to differences between myosin isoforms. Alternatively, this would be consistent with a series elastic element at the base of the lever-arm that is extended under load while the lever-arm itself behaves more like a rigid rod. The stiffness would then be expected to change with the reciprocal of the squared lever-arm length ($L_{(SMS1)}{}^{-2}/L_{(MVS1)}{}^{-2} \approx 9$; here $\kappa_{SMS1}/\kappa_{MVS1} \approx 2.3$) and the distance parameter to change proportionally to the lever-arm length ($L_{(MVS1)}/L_{(SMS1)} \approx 3$; here $d_{1(MVS1)}/d_{1(SMS1)} \approx 1.6$). The difference in distance parameter and stiffness between MVS1 and SMS1 was even less pronounced than that. However, we would expect the distance parameter for MVS1 to be $d_{1(MVS1)}/d_{1(SMS1)} \sim 0.5(L_{(MVS1)}/L_{(SMS1)}) \approx 1.5$ if the basal series elastic element were about twice as far from the pivot for MVS1 compared with SMS1. Then we would expect $\kappa_{SMS1}/\kappa_{MVS1} \approx 1/4(L_{(SMS1)}{}^{-2}/L_{(MVS1)}{}^{-2}) \approx 2.3$, which agrees well with the data.

We propose that the processive movement of mouse myosin-V is achieved as follows: head 1 binds to actin with ADP.Pi in its catalytic site, phosphate leaves and a 20 nm working stroke is produced (Fig. 5; state A). Head 2 then undergoes a diffusive search along the actin filament and binds preferentially to the actin monomer that presents the least azimuthal distortion (36 nm downstream from head 1) (Fig. 5; state B). Binding of head 2 causes intramolecular strain, stored as elastic strain energy in some element in each head. The mechanical coupling of the two elastic elements has a synchronizing effect on the chemo-mechanical cycles because conformational changes on one head directly affect strain-dependent kinetics on the other head. A pulling force acting on head 2 slows down loss of product and conformational change, arresting the cycle of that head in an early stage of attachment. At the same time, a pushing force on head 1 initiates events that accelerate transition into detachment, such as a second conformational change (of 5 nm) in head 1 followed by loss of ADP, binding of ATP and dissociation of head 1 (Fig. 5; state C). The detachment of head 1 releases strain, leaving head 2 as the single bound head (Fig. 5; state A, heads swapped), which will now complete the 20 nm working stroke. Because this head had been held back in an early stage of attachment, the chances of its premature detachment, before the free head rebinds, are minimized. Key to the mechanism are the following features: (1) the myosin-V working stroke is not commensurate with the helical repeat so that two-headed binding causes intramolecular strain; (2) elastic elements storing the strain energy in both heads are mechanically coupled; this coordinates the biochemical cycles 'out of phase'; (3) the attached state of a single head consists of two successive phases, the first one being load-dependent, and detachment is only allowed from the second phase. This increases the number of forward steps per processive run in two ways: first, by increasing the probability of the rear head detaching first; second, by decreasing the probability that both heads detach during the same time period.

METHODS

Protein preparations, solutions and optical trapping conditions. Bacculo-virus-expressed mouse myosin-V fragment S1 (MVS1)[30,39] and myosin S1 prepared from chicken gizzard muscle (SMS1)[32] were prepared as described previously. MVS1 was composed of the motor domain and neck region including all six light-chain binding motifs. The protein was active in *in vitro* motility assays and moved actin at a velocity of ~0.3 μm s^{-1}. Rhodamine-phalloidin-labelled F-actin and *N*-ethyl maleimide (NEM)-modified rabbit myosin were prepared by standard methods[29]. We used an optical tweezers transducer that was built around a Zeiss Axiovert microscope[28,29]. Experiments were performed using flow cells made from a microscope slide and pieces of coverslip[29]. Glass microspheres (2.1-μm diameter) were applied to the coverslip surface as a suspension in 0.1% v/w nitrocellulose/amyl acetate. The nitrocellulose surface was precoated with 10 μg ml^{-1} BSA (Sigma-Aldrich, Dorset, UK). Then, MVS1 was allowed to bind to the coverslip surface, using 10–50 ng ml^{-1} of protein in buffered salt solution (containing in mM: 25 KCl, 25 imidazole, 4 $MgCl_2$, 1 EGTA; pH 7.4; 23 °C). When SMS1 was used, myosin was applied straight to the nitrocellulose surface without precoating with BSA. Next, this solution was replaced with one containing rhodamine-phalloidin-labelled actin filaments and 1.1 μm polystyrene beads that had been precoated with NEM-modified myosin. The buffered salt solution was supplemented with (in mM): 2 creatine phosphate, 20 dithiothreitol, 0.003–0.02 ATP; and (in mg ml^{-1}): 1 creatine phosphokinase, 0.5 BSA, 3 glucose, 0.1 glucose

oxidase, 0.02 catalase. In the experiments, a single actin filament (average filament length ~4 μm) was attached at either end to a 1.1-μm polystyrene bead held in optical tweezers and positioned in the vicinity of a stationary glass microsphere. Interactions between actin and the surface bound myosin-V were monitored by casting the image of the polystyrene beads onto two 4-quadrant photodetectors. With the actin filament held taut, but in the absence of myosin binding, the r.m.s. amplitude of brownian motion was: $(k_bT/2\kappa_{trap})^{0.5} \approx 12$ nm (where k_bT = thermal energy, κ_{trap} = optical tweezers stiffness = 0.015–0.02 pN nm^{-1}). When myosin bound to actin, the motion of the beads parallel to the filament axis was restrained by an additional stiffness, κ_{add} making the total system stiffness $\kappa_{tot} = 2\kappa_{trap} + \kappa_{add}$, which reduced the r.m.s. amplitude to $(k_bT/\kappa_{tot})^{0.5}$. Brownian motion showed a lorentzian power–density distribution with a roll-off frequency $f_c = \kappa_{tot}/2\pi\beta \approx 500$ Hz (where $\beta = 6\pi\eta r$; η = solution viscosity, r = combined bead radii = 1.1 μm). To improve time resolution with which myosin binding could be detected we oscillated the position of one laser tweezer at a frequency of $f = 1$ kHz, r.m.s. amplitude $A_0 = 35$ nm, and measured the transmission of this motion to the bead in the other trap (Fig. 2a). The effect of viscous damping and series elastic elements caused the amplitude of the movement of the bead in the other trap to be smaller and drop strongly upon myosin binding ($A_r = (A_0\kappa_{trap})/(\kappa_{tot}^2 + (2\beta 2\pi f)^2)^{0.5}$; where $\kappa_{tot} = 2\kappa_{trap} + \kappa_{add}$ and during myosin attachment κ_{add} increases from zero to about 0.2 pN nm^{-1}). By oscillating one optical tweezer in this way it was possible to detect myosin binding from the change in amplitude of the 1-kHz signal with a time resolution of ~1 ms (using discrete Fourier transformation of the 1-kHz signal over a running time window of 1 ms)[32]. Data were sampled at 10 kHz. All experiments were performed at 23 °C.

Application of load. We recorded the amplitude of the 1-kHz signal, transmitted to the bead in the stationary trap (Fig. 2a; right bead), using an analogue r.m.s.-to-d.c. converter circuit[32]. In brief, myosin binding was detected by thresholding changes in amplitude of the r.m.s. value of the 1-kHz signal (value below threshold for a minimum of ~3 ms) to produce a digital signal. We then used the digital signal to change the position of both optical traps. To apply load, both traps were moved by a distance dx_{trap} in parallel to the actin filament axis to give a force, $F = 2\kappa_{trap}.\Delta x$ (with κ_{trap} = stiffness of a single trap; $\Delta x = x_{trap} - x_{bead}$; x_{trap} = position of one particular trap; and x_{bead} = position of bead held in that trap). Following detection of crossbridge detachment, the traps were returned to their rest position, again with a time delay of ~3 ms. For analysis, we only took events with a minimum lifetime of 20 ms into account. Although the average force applied by the 1-kHz sinusoid is zero during the lifetimes of binding events (>20ms), we cannot exclude some contribution to the load-dependent changes in rate constants, as the measured effect of load on the kinetics was non-linear.

Calculation of mean lifetimes, ensemble averaging and statistics. The mean lifetime of binding events, t_{50}, was given by $t_{50} = (t_{av} - t_{min})$, where t_{av} is the measured average lifetime for all events lasting longer than t_{min} (here 20 ms)[31]. The mean lifetimes are given together with their theoretical standard error (s.e.), which was defined as s.e. = $t_{50}.(n^{-0.5})$ (ref. 31). For ensemble averaging, we aligned individual attachment events to the time point of their beginning or end[13,32]. In brief, we determined the time points by thresholding the changes in amplitude of the transmitted 1-kHz signal (Fig. 2a). All identified attachment events with lifetime t_n were then made to be of the same duration t by extending short events by time $t - t_n$, keeping the level reached at the end of the event during the extra time t–t_n. Individual attachment events were then synchronized, either to the time point of beginning or the time point of end, and averaged, as illustrated in the cartoon in Fig. 3 (ref. 32). Amplitudes and transition rates of phase 1 and 2 of the working stroke (k_1 and k_2) were determined by exponential fitting to the data. The complex time course at the onset and end of the ensemble-averaged displacements under load (Fig. 3b, c) can be explained as follows: the onset of load (push or pull) initiates two events; first, the rapid extension or compression of an elastic element with stiffness κ_{com}, composed of κ_{con}, connecting the actin filament to the handle beads, and κ_{myo}, the attached crossbridge ($\kappa_{con} \approx 0.2$–0.4 pN nm^{-1}, $\kappa_{myo} \approx 0.2$ pN nm^{-1}). This causes an additional displacement of the bead in the direction of the applied load of $F/\kappa_{com} \approx 12$–$15$ nm, until the system settles and near constant-load conditions are reached after ~40 ms (red curves in Fig. 3b, c; see ref. 32); second, the second step of the working stroke. The amplitude and direction of that slower exponential component, k_1, are independent of the applied load, but the kinetics are accelerated when a push is applied, and slowed down when the crossbridge is pulled. This is expected for a strain-dependent conformational change, in contrast to the extension of a passive elastic element. We interpret the time course of the ensemble averaged record at the end of attachment events as follows: after detection of crossbridge detachment, the tweezers are repositioned with a time delay of about 3 ms. During the transition time of about 10 ms to zero load, a rapid displacement in the direction of applied load was observed (in the ensemble average), before the beads return to resting position (Fig. 3b, c; red lines, preceding crossbridge detachment). The kinetics of this fast displacement are independent of the direction of load. They can be explained by the relaxation time of the unbound bead–actin–bead dumbbell moving towards the centre of the optical tweezers after crossbridge detachment ($\tau = 6\pi\eta r/\kappa_{trap} \approx 2$–$3$ ms).

The ensemble averages in Fig. 3 also show that the initial displacement following attachment occurs too quickly for its kinetics to be separated from the timing errors made in the alignment of the attachment events ($\tau \approx 2$ ms). When fitting exponentials to resolve amplitude and kinetics of the two phases of the working stroke, which follow the initial displacement, we ignored the first 5 ms from the time point of beginning and end of the ensemble averages. We calculated the standard error of fitted exponentials as s.e.m. = $(\sum(y_i - f(x_i))^2/(n-1))^{0.5}$, with y_i denoting the data points, $f(x_i)$ the value calculated from the regression model and $(n-1)$ the number of degrees of freedom. The correlation coefficient of the fits was calculated as $r = ((S_t - S_r)/S_t)^{0.5}$, with $S_t = \sum(y_{av} - y_i)^2$; y_{av} = mean value of y_i, and $S_r = \sum(y_{av} - f(x_i))^2$.

BIND identifier. One BIND identifier (www.bind.ca) is associated with this manuscript: 316291.

ACKNOWLEDGEMENTS

We thank E. Harvey for technical assistance, J. A. Hammer III for kindly supplying the MV clone, J. E. Molloy, J. Howard and M. A. Geeves for helpful discussions and critical reading of the manuscript, and MRC, The Royal Society, BBSRC and NIH for grant support.

COMPETING FINANCIAL INTERESTS

The authors declare that they have no competing financial interests.

Received 8 April 2005; accepted 25 July 2005
Published online at http://www.nature.com/naturecellbiology.

1. Reck-Peterson, S., Provance, D. W., Mooseker, M. S. & Mercer, J. A. Review: Class V myosins. *Biochim. Biophys. Acta* **1496,** 36–51 (2000).
2. Sellers, J. R. *Myosins* (Oxford University Press, Oxford, 1999).
3. Cheney, R. E. *et al*. Brain Myosin-V is a two-headed unconventional myosin with motor activity. *Cell* **75,** 13–23 (1993).
4. Miller, .E. & Sheetz, M. P. Characterization of myosin-V binding to brain vesicles. *J. Biol. Chem.* **275,** 2598–2606 (2000).
5. Vale, R. D. Myosin V motor proteins: marching stepwise towards a mechanism. *J. Cell Biol.* **163,** 445–450 (2003).
6. Mehta, A. D. *et al*. Myosin-V is a processive actin-based motor. *Nature* **400,** 590–593 (1999).
7. Rief, M. *et al*. Myosin-V stepping kinetics: A molecular model for processivity. *Proc. Natl Acad. Sci*. **97,** 9482–9486 (2000).
8. Sakamoto, T., Amitani, I., Yokota, E. & Ando, T. Direct observation of processive movement by individual myosin-V molecules. *Biochem. Biophys. Res. Comm.* **272,** 586–590 (2000).
9. Sakamoto, T. *et al*. Neck length and processivity of myosin-V. *J. Biol. Chem.* **278,** 29201–29207 (2003).
10. Yildiz, A. *et al*. Myosin-V walks hand over hand: single fluorophore imaging with 1.5nm localisation. *Science* **300,** 2061–2065 (2003).
11. Forkey, J. N., Quinlan, M. E., Shaw, M. A., Corrie, J. E. & Goldman, Y. E. Three dimensional structural dynamics of myosin-V by single-molecule fluorescence polarisation. *Nature* **422,** 399–404 (2003).
12. Walker, M. *et al*. Two-headed binding of a processive myosin to F-actin. *Nature* **405,** 804–807 (2000).
13. Veigel, C., Wang, F., Bartoo, M. L., Sellers, J. R. & Molloy, J. E. The gated gait of the processive molecular motor myosin-V. *Nature Cell Biol*. **4,** 59–65 (2002).
14. Ali, M. Y. *et al*. Myosin-V is a left-handed spiral motor on the right-handed actin helix. *Nature Struct. Biol*. **9,** 464–467 (2002).
15. Tanaka, H. *et al*. The motor domain determines the large step of myosin V. *Nature* **415,** 192–195 (2002).
16. Schnitzer, M. J. & Block, S. M. Statistical kinetics of processive enzymes. *Cold Spring Harb. Symp. Quant. Biol.* **60,** 793–802 (1995).
17. Kolomeisky, A. B. & Fisher, M. E. A simple kinetic model describes the processivity of myosin-V. *Biophys. J.* **84,** 1642–1650 (2003).
18. Lan, G. & Sun, S. X. Dynamics of myosin processivity. *Biophys. J.* **88,** 4107–4117 (2005).
19. Coureux, P. D., Sweeney, H. L. & Houdusse, A. Three myosin-V structures delineate essential features of chemo-mechanical transduction. *EMBO J.* **23,** 4527–4537 (2004).

20. Purcell, T. J., Morris, C., Spudich, J. A. & Sweeney, H. L. Role of the lever arm in the processive stepping of myosin-V. *Proc. Natl Acad. Sci. USA* **92,** 14159–14164 (2002).
21. Huxley, A. F. Muscle structure and theories of contraction. *Progr. Biophys. Biophys. Chem.* **7,** 255–318 (1957).
22. De La Cruz, E. M., Wells, A. L., Rosenfeld, S. S., Ostap, E. M. & Sweeney, H. L. The kinetic mechanism of myosin-V. *Proc. Natl Acad. Sci.* **96,** 13726–13731 (1999).
23. Baker, J. E. *et al.* Myosin-V processivity: multiple kinetic pathways for head-to-head coordination. *Proc. Natl Acad. Sci. USA* **101,** 5542–5546 (2004).
24. Clemen, A. E. *et al.* Force dependent stepping kinetics of myosin-V. *Biophys. J.* **88,** 4402–4410 (2005).
25. Moore, J. R., Krementsova, E. B., Trybus, K. M. & Warshaw, D. M. Myosin-V exhibits a high duty cycle and large unitary displacement. *J. Cell Biol.* **155,** 625–635 (2001).
26. Uemura, S., Higuchi, H., Olivares, A. O., DeLaCruz, E. M. & Ishiwata, S. Mechanochemical coupling of two substeps in a single myosin-V motor. *Nature Struct. Biol.* **11,** 877–883 (2004).
27. Rosenfeld, S. S. & Sweeney, H. L. A model for myosin-V processivity. *J. Biol. Chem.* **279,** 40100–40111 (2004).
28. Molloy, J. E., Burns, J. E., Kendrick-Jones, J., Tregear, R. T. & White, D. C. S. Movement and force produced by a single myosin head. *Nature* **378,** 209–212 (1995).
29. Veigel, C., Bartoo, M. L., White, D. C. S, Sparrow, J. C. & Molloy, J. E. The stiffness of rabbit skeletal, acto-myosin crossbridges determined with an optical tweezers transducer. *Biophys. J.* **75,** 1424–1438 (1998).
30. Wang, F. *et al.* Effect of ADP and ionic strength on the kinetic and motile properties of recombinant mouse myosin-V. *J. Biol. Chem.* **275,** 4329–4335 (2000).
31. Veigel, C. *et al.* The motor protein myosin-I produces its working stroke in two steps. *Nature* **398,** 530–533 (1999).
32. Veigel, C., Molloy, J. E., Schmitz, S. & Kendrick-Jones, J. Load-dependent kinetics of force production by smooth muscle myosin measured with optical tweezers. *Nature Cell Biol.* **5,** 980–986 (2003).
33. Howard, J. *Mechanics of Motor Proteins and the Cytoskeleton* (Sinauer Associates, Inc., Sunderland, 2001).
34. Lymn, R. W. & Taylor, E. W. Mechanism of adenosine triphosphate hydrolysis by actomyosin. *Biochemistry* **10,** 4617–4624 (1971).
35. Burgess, S. *et al.* The prepower stroke conformation of myosin-V. *J. Cell Biol.* **159,** 983–991 (2002).
36. Whittaker, M. *et al.* A 35-Å movement of smooth muscle myosin on ADP release. *Nature* **378,** 748–751 (1995).
37. Berger, C. E. M, Fagnant, P. M., Heizmann, S., Trybus, K. M. & Geeves, M. A. ADP binding induces and asymmetry between the heads of unphosphorylated myosin *J. Biol. Chem.* **276,** 23240–23245 (2001).
38. Lombardi, V. *et al.* Elastic distortion of the myosin head and repriming of the working stroke in muscle. *Nature* **374,** 553–555 (1995).
39. Cheney, R. E. Purification and assay of myosin-V. *Methods Enzymol.* **298,** 3–18 (1998).
40. Mehta, A. D., Finer, J. T. & Spudich, J. A. Stiffness of muscle myosin. Detection of single-molecule interactions using correlated thermal diffusion. *Proc. Natl Acad. Sci. USA* **94,** 7927–7931 (1997).
41. Tyska, M. J. *et al.* Two heads of myosin are better than one for generating force and motion. *Proc. Natl. Acad. Sci. USA* **96,** 4402–4407 (1999).